A grid-tie inverter topology with maximum power extraction from two PV arrays

Iván Patrao* (ivpather@upvnet.upv.es), Gabriel Garcerá (ggarcera@eln.upv.es), Emilio Figueres (efiguere@eln.upv.es), Raúl González-Medina (raugonme@upvnet.upv.es)
Grupo de Sistemas Electrónicos Industriales del Departamento de Ingeniería Electrónica, Universitat Politécnica de Valencia, Camino de Vera s/n, 46022 Valencia, España.

*Corresponding author. e-mail address: ivpather@upvnet.upv.es. Phone number: +34 963 87 96 06.

***Abstract* — This paper presents a transformerless topology for a grid tied single-phase inverter capable of performing the simultaneous maximum power point tracking of two independent and series connected photovoltaic sources. This topology is derived from the Neutral Point Clamped multilevel inverter in half-bridge configuration. The use of a half-bridge topology reduces the leakage current to very low values, whereas the multilevel topology presents an output voltage quality similar to that of a full-bridge inverter. In order to simultaneously track the maximum power of both photovoltaic sources a Generation Control Circuit is used. With this topology it is possible to improve the performance of the converter under partial shadowing conditions, very common in photovoltaic facilities operating in residential areas. A *5 kW* prototype of this topology has been implemented and tested in the laboratory.**

I. INTRODUCTION

Photovoltaic (PV) and renewable energy sources (RES) have experimented a great development in recent years [1], mainly due to the growing concern about climate change and the oil price increase, which has led many countries to adopt new regulations to promote this kind of energy.

In power converters for RES, and especially in grid-connected PV inverters, efficiency and cost are key factors [2]. Many of these inverters use an isolation transformer between the PV panels and the grid, but these low frequency transformers are bulky and expensive. Furthermore, they produce additional losses [3;4]. Using a two stage topology with high frequency isolation can reduce the size and price of the transformer, but the overall efficiency of the system is reduced, since at least two cascaded power stages are used (dc-dc + inverter). Therefore, a large number of transformerless inverter topologies have been proposed in the last years [5]. These inverters are cheaper, more compact and more efficient [4;6] than their counterparts.

Regarding the size of grid-connected photovoltaic inverters, a change of paradigm has been observed in the last few years. Large central inverters (above *100kW*) are being substituted by string inverters around a few kilowatts that process the energy of a small group of photovoltaic panels, improving the maximum power point tracking (MPPT) of a photovoltaic system, as the modules could be exposed to different solar irradiation levels. In this context, the use of single-phase inverters up to *5kW* has gained great interest [7], especially in residential areas, to solve problems like different orientation of photovoltaic panels, partial shadows or accumulated dust. Furthermore, the possibility of producing energy close to the consumption points by means of a large number of small distributed energy generators has raised many expectations [8-10].

The distributed generation scenario is promoting the research about power converters to reduce the impact of the partial shadowing problem [11;12]. Thus, module-integrated converters (MIC), microinverters and multi-input string inverters are being developed. However, MICs and microinverters usually require cascade conversion stages that decrease the efficiency and make the system more complex. Therefore, string inverters are most commonly used. Besides, there are some topologies of string inverters that reduce the partial shadowing problem, by means of independent control of the multiple photovoltaic inputs. The principle of serial connection of PV strings with maximum power extraction from each individual string by means of a single inverter has raised a high interest in the last years [13-15].

The grid-connected PV inverter presented in this paper is a *5kW* multi-input transformerless string inverter with simultaneous MPPT of two PV sources. This topology, called NPC+GCC, solves the typical issues of transformerless PV inverters related to leakage currents from the PV panels to ground due to high frequency common mode voltages [6;16]. Moreover, the auxiliary DC-DC converter used in this topology (the GCC circuit) exhibits low losses, since it only processes the power difference between both PV strings. Therefore, the efficiency of this double-stage converter is similar to that of a single-stage inverter.

II. THE COMMON MODE VOLTAGE PROBLEM

Photovoltaic modules have a very large conductive surface which may have a large parasitic capacitance to ground under certain operating conditions (e.g. humidity, dust or in some kinds of facility), with capacitance values up to *150nF/kW* for crystalline-silicon cells and up to *1μF/kW* for thin-film cells [6]. The parasitic capacitances between ground and both terminals of the PV source, $C_{parasitic1}$ and $C_{parasitic2}$, are depicted in the single-phase transformerless grid connected PV inverter of figure 1.

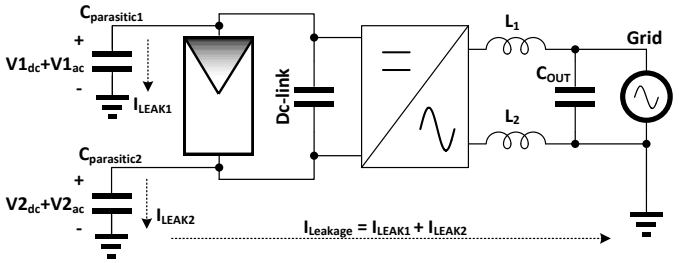

Fig. 1. Common mode leakage currents in a transformerless grid connected PV inverter

The AC voltages at the PV module terminals (V1 and V2) produce leakage currents to ground through the parasitic capacitances $C_{parasitic1}$ and $C_{parasitic2}$. The currents induced by those voltages can be classified into differential mode currents and common mode currents. The differential mode voltage, V_{DM}=V1-V2, generates a current that flows from one pole of the PV modules to the other one; this current does not generate leakage problems. The common mode voltage, V_{CM}=(V1+V2)/2, generates a leakage current ($I_{Leakage}$) that flows from the poles of the PV source, through the ground of the PV source, to the ground of the grid, which is connected to the neutral of a single-phase utility grid [13].

This current may produce problems in the photovoltaic system (e.g. protections triggering, efficiency degradation, safety problems, and electromagnetic compatibility problems) [6;16]. When using the newest technologies of photovoltaic cells, like back-contact cells, amorphous-Silicon thin-film cells (a-Si) or cadmium telluride cells (CdTe), the leakage current can produce irreversible effects on the PV cells, affecting the efficiency of the overall system permanently [6].

If the common mode voltage at the PV module is purely sinusoidal with an RMS value V_{CM_RMS}, and both parasitic capacitances are similar ($C_{parasitic1} \approx C_{parasitic2} \equiv C_{parasitic}$), the RMS value of the leakage current can be derived as (1), where $C_{parasitic\_eq}=2 \cdot C_{parasitic}$, and f denotes the frequency of the common mode voltage. As the leakage current is proportional to the frequency of the common mode voltage, the most disturbing common mode voltages are those containing switching frequency harmonics.

Therefore, current research on transformerless inverters focuses on finding new topologies and modulation strategies which have an almost DC or low frequency common mode voltage, thus generating very low leakage currents [5;17].

$$I_{LEAK\_RMS} = 2 \cdot \pi \cdot f \cdot C_{parasitic\_eq} \cdot V_{CM\_RMS} \qquad (1)$$

III. The Partial Shadowing Problem

A string is a group of photovoltaic modules connected in series, where the total PV source voltage is the sum of the individual modules voltages, whereas all modules share the same current. When the solar irradiation level at one individual module of the string decreases, its maximum current decreases too, limiting the current in the whole string, because of the series connection. When limiting the current of the string it is also being limited the maximum power of the PV source, so that it is impossible to have all the modules working at its maximum power point (MPP) [18]. In these conditions, the voltage-power curve of the PV source presents some local MPPs, all of them with a power lower than the sum of the achievable MPPs of the individual modules.

To reduce the partial shadowing problem, many string inverters use as a first stage a dc-dc converter (e.g. a boost converter) for each module or for a small group of series connected modules. It is worth pointing out that the smaller the number of interconnected PV modules, the better is the MPP tracking under partial shadowing. The dc-dc converter performs the maximum power point tracking (MPPT) of each module or group of modules. The outputs of the dc-dc converters are connected in parallel to the grid connected inverter. However, the overall efficiency and reliability of the whole power conversion system is affected, as it is formed by power converters connected in series [19].

IV. Proposed Topology

The proposed topology for a transformerless inverter working from two PV sources connected in series is called NPC+GCC, and it is formed by a Neutral Clamped Inverter (NPC) in a half-bridge configuration and a Generation Control Circuit (GCC) running together and sharing the input stage.

The Generation Control Circuit is an electronic power converter based on the classical buck-boost dc-dc converter, with its output connected to the midpoint of both PV sources, as it is shown in figure 2.a. It is composed by two semiconductor switches (IGBT1 and IGBT2) in series and one inductor (Lgcc) connected between the switches and the midpoint of the PV source [20]. Note that the GCC needs a splitted input dc-link.

This circuit manages the voltage at the midpoint of the dc-link, allowing the operation of each PV string at a different current-voltage point. This feature avoids the partial shadowing problem, in which the maximum current of the most shaded photovoltaic module limits the current of the string.

The main advantage over other dc-dc converter topologies is that the GCC only manages the power difference between both strings instead of the full power, thus reducing the overall power losses. The requirement of a splitted dc-link it is not a disadvantage for this topology, because the topology of the NPC inverter requires that kind of dc-link, which can be shared with the GCC.

The NPC half-bridge inverter consists of four active switches connected in series (IGBT1 to IGBT4) and two clamping diodes (D1 and D2), connected as shown in figure 2.b. The topology provides three levels at the output voltage, like a full-bridge topology with unipolar pulse with modulation (PWM). The output LC filter (L_{npc}, C_{out}) provides the required attenuation of the switching frequency harmonics of the grid injected current, allowing the connection to the grid.

On one hand, the NPC half-bridge has a similar structure to that of a classical half-bridge, since it requires the connection of the grid neutral to the midpoint of the dc-link, but the NPC provides a better efficiency and a smaller current ripple. Furthermore, the NPC half-bridge has a low ripple-low frequency common mode voltage, thus reducing the leakage current. On the other hand, the NPC topology has a performance similar to that of the full-bridge with unipolar PWM, since it has 3 output voltage levels and a similar derivative of the output voltage (dv/dt) before filtering. Consequently, the output filter design of the NPC half-bridge is similar to that of a unipolar PWM full-bridge. As it was reported in [21], the grid connected NPC half bridge inverter has small leakage currents, because the common mode voltage has only low frequency (line frequency) components.

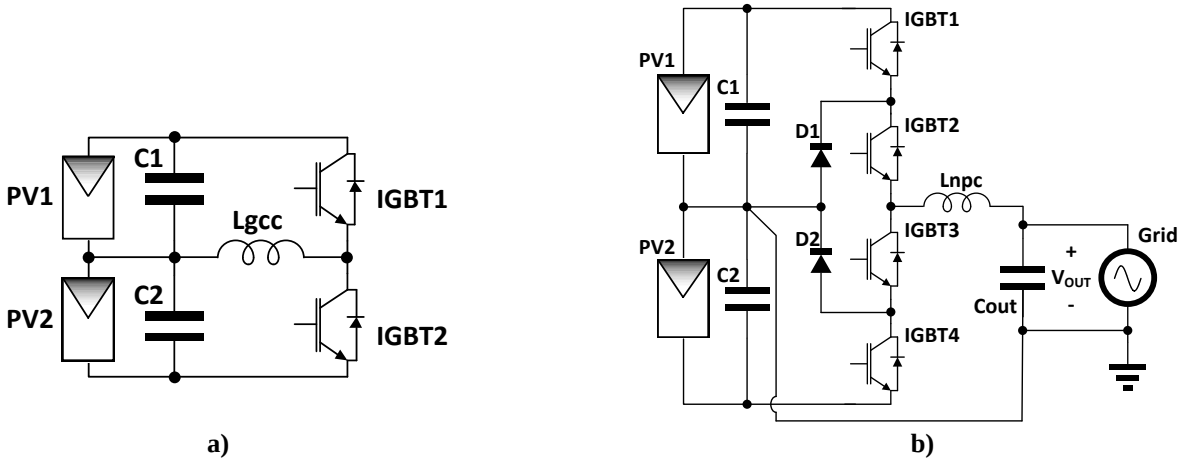

Fig. 2. a) Generation control circuit (GCC), b) Neutral point clamped half-bridge inverter (NPC).

The modulation technique used by the NPC inverter of this work is the sinusoidal PWM, using two triangular carrier waveforms with in-phase disposition (IPD). The concept of the IPD PWM modulator used by the NPC inverter is shown in figure 3.a. The modulator is composed by a pair of comparators and two in-phase carrier signals with different offset voltages. A schematic representation of the gate signals and of the resulting three-level output voltage, V_{out}, is shown in figure 3.b.

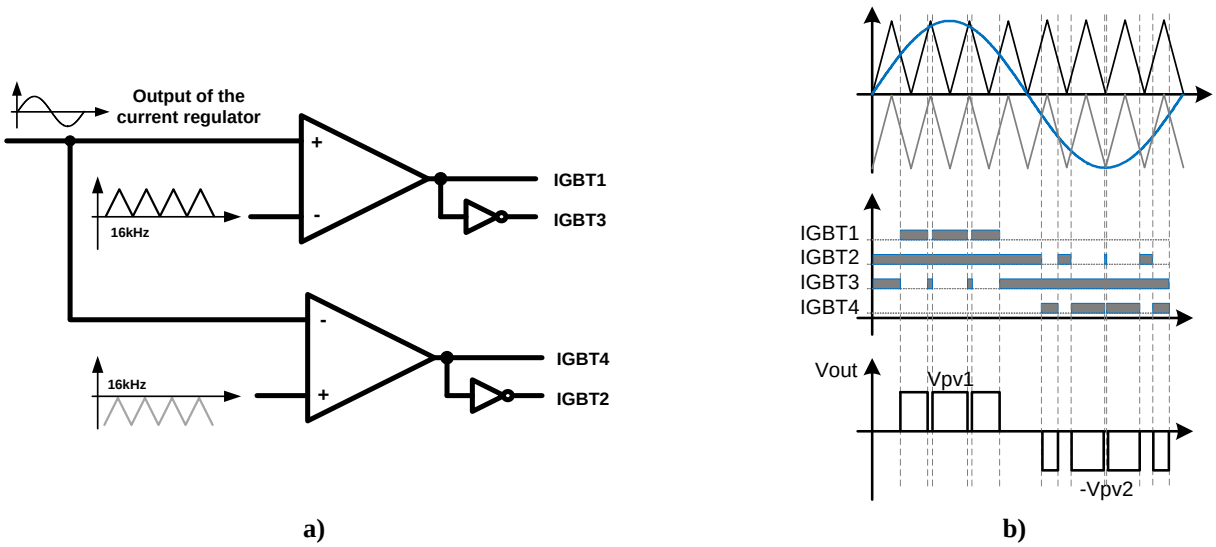

Fig. 3. a) Concept of the IPD PWM modulator of the NPC inverter, b) Schematic representation of the gate signals and of the output voltage of the NPC inverter

The proposed topology, shown in figure 4.a, is composed by a GCC converter and an NPC inverter. Switches IGBT1 to IGBT4 and D1-D2 make up the NPC inverter, whereas the GCC converter is made of IGBT5 and IGBT6. Both the GCC and the NPC

need a midpoint at the dc-link, so that they can work together, leading to a new high-efficiency transformerless inverter topology with independent MPPT of its two input voltages, avoiding the use of cascaded converters processing the whole PV power. The NPC inverter injects the available power to the grid, whereas the GCC converter manages the current unbalance at the input, processing a small power.

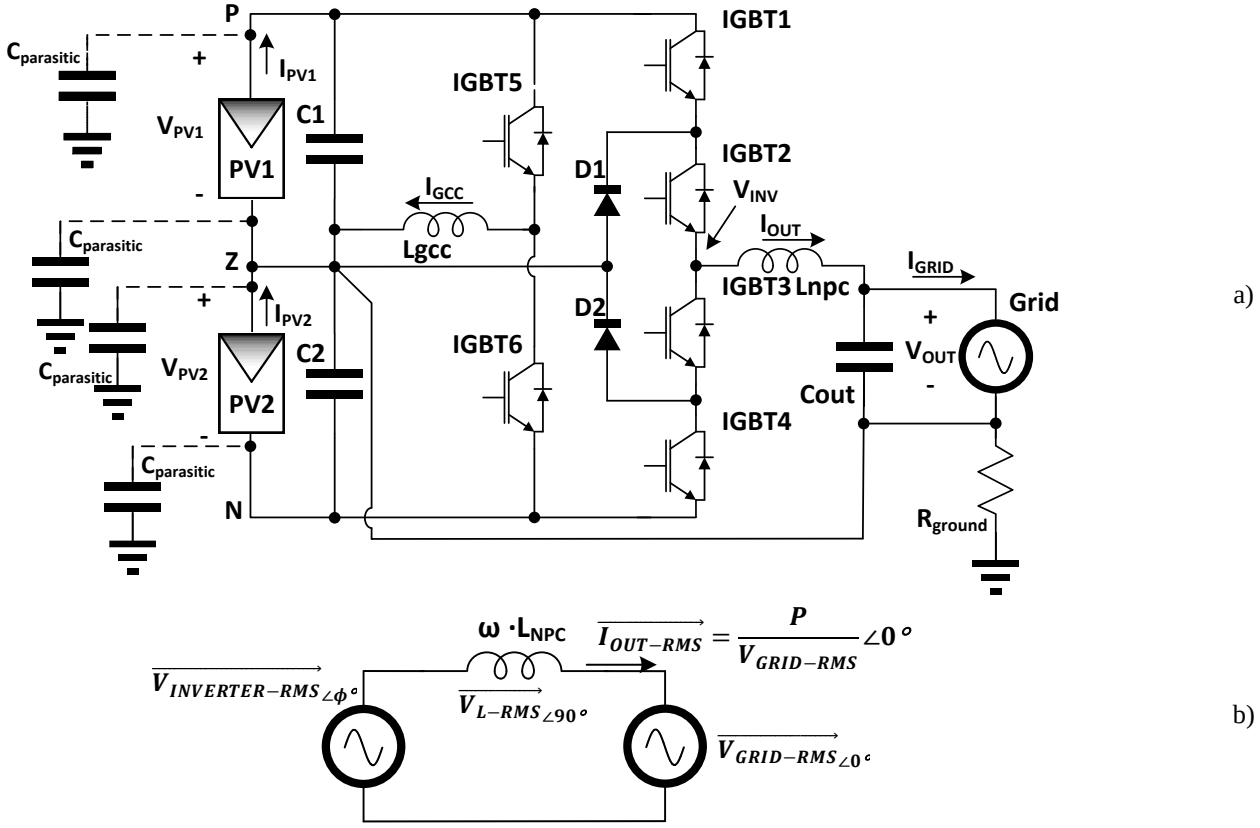

Fig. 4. Proposed topology (NPC+GCC). a) Circuit schematic; b) equivalent circuit of the inverter at the grid fundamental frequency for calculation of the L_{NPC} inductance.

The inductance value of the NPC inverter inductor, L_{NPC}, has been calculated based on the circuit of figure 4.b, which depicts the equivalent circuit of the inverter at its fundamental frequency (*50 Hz*), being $V_{INVERTER}$ the fundamental component of the voltage generated by the inverter, and $\omega = 2 \cdot \pi 50\ Hz$. All the phasors correspond to fundamental frequency components. The grid voltage has been chosen as the phase origin of the phasors.

$$\vec{V}_{INV-RMS} = \vec{V}_{GRID-RMS} + \vec{V}_{L-RMS} \rightarrow \vec{V}_{INV-RMS} = \vec{V}_{GRID-RMS} + \frac{j \cdot \omega \cdot L_{NPC} \cdot P}{V_{GRID-RMS}} \quad (2)$$

$$V_{INV-RMS} = \sqrt{{V_{GRID-RMS}}^2 + \left(\frac{\omega \cdot L_{NPC} \cdot P_{MAX}}{V_{GRID-RMS}}\right)^2} \quad (3)$$

The condition (4) must be fulfilled in order to make the inverter to work in the linear modulation region, where $\min(V_{PV1}, V_{PV2}) = V_{PV\text{-}min}$ represents the minimum expected operation value of the voltage at any of the strings.

$$V_{INV-RMS} = \sqrt{{V_{GRID-RMS}}^2 + \left(\frac{\omega \cdot L_{NPC} \cdot P_{MAX}}{V_{GRID-RMS}}\right)^2} \leq \frac{min(V_{PV1}, V_{PV2})}{\sqrt{2}} \quad (4)$$

From (4), the maximum value of L_{NPC} can be derived:

$$L_{NPC} \leq \frac{V_{GRID-RMS} \cdot \sqrt{\frac{V_{PV-min}^2}{2} - V_{GRID-RMS}{}^2}}{\omega \cdot P_{MAX}} \quad (5)$$

The following values have been used for the calculation of the inductor value. Note that this is a conservative calculation because for *5 kW* the strings will have a higher value than *370 V*.

- $V_{GRID-RMS} = 230\ V$
- $V_{PV-min} = 370\ V$
- $\omega = 2 \cdot \pi 50 = 314.16\ rad/s$
- $P_{MAX} = 5\ kW$

Thus, the maximum value for the output inductor is $L_{NPC} < 18\ mH$. The selected value for the output inductance is *2 mH*, much lower than the calculated limit.

The value of the GCC inductor is calculated to limit the current ripple in that inductance. It has been chosen a value of *16 kHz* for the switching frequency, in order to minimize magnetic hysteresis losses in the core, thus maximizing the converter efficiency. The price that must be paid for this relatively low switching frequency is the inductor size.

The maximum value of the current ripple, ΔI_{GCC}, in the GCC inductor is selected to be 25 % of the maximum value of the inductor current dc value, I_{GCC}, which is the short-circuit current of one PV string: $I_{GCC-MAX} = 8\ A$. Therefore, the value of L_{GCC} has been calculated to obtain a maximum value of the current ripple $\Delta I_{GCC-MAX} = 2\ A$. The equation used to calculate the value of the inductor is (6).

$$L_{GCC} = \frac{V_{PV-MPP}}{\Delta I_{GCC-MAX} \cdot f_{SW}} \quad (6)$$

The design of the GCC inductor has been performed by means of Micrometals© software. With a core type T400-40D from Micrometals© and 550 turns the resulting inductance at *8 A* is: $L_{GCC} = 14.62\ mH \approx 15\ mH$.

The power losses in the GCC have been calculated, starting from the knowledge of its operation point and both the IGBTs and the GCC inductor datasheets. Three different unbalance scenarios have been taken into account for calculating the power losses in the GCC, with a constant output power and different power unbalances at the input. The results, shown below, demonstrate how the losses in the GCC strongly depend on the power unbalance between both strings, being the worst case that with a higher unbalance.

Balanced generation:

- $V_{PV1} = 468.5\ V;\ I_{PV1} = 3.25\ A$
- $V_{PV2} = 468.5\ V;\ I_{PV2} = 3.25\ A$
- $I_{GRID} = 12.93\ A_{rms}\ (P_{GRID} = 3\ kW)$
- *Power losses in the GCC converter (IGBT5, IGBT6 and GCC inductor): 4.1 W*

Unbalanced generation:

- $V_{PV1} = 452.3\ V;\ I_{PV1} = 4.58\ A$
- $V_{PV2} = 482.1\ V;\ I_{PV2} = 2.03\ A$
- $I_{GRID} = 12.93\ A_{rms}\ (P_{GRID} = 3\ kW)$
- *Power losses in the GCC converter (IGBT5, IGBT6 and GCC inductor): 26.4 W*

Severely unbalanced generation:

- $V_{PV1} = 428\ V;\ I_{PV1} = 6.05\ A$
- $V_{PV2} = 490.9\ V;\ I_{PV2} = 0.98\ A$
- $I_{GRID} = 12.93\ A_{rms}\ (P_{GRID} = 3\ kW)$
- *Power losses in the GCC converter (IGBT5, IGBT6 and GCC inductor): 59 W*

The GCC stage can be compared with a usual alternative providing double MPPT at the input like the double-boost converter (+ NPC half-bridge) depicted in figure 5. In that topology the input voltage of each boost converter is lower than that of the NPC+GCC converter and, therefore, the inductance value is also lower. Nevertheless, two equal inductors are required instead of a single one. Besides, the double-boost requires a higher number of semiconductors and sensors: a voltage sensor for each PV source, additionally to a voltage sensor for the input voltage of the NPC inverter, and a current sensor for the current delivered by each PV source.

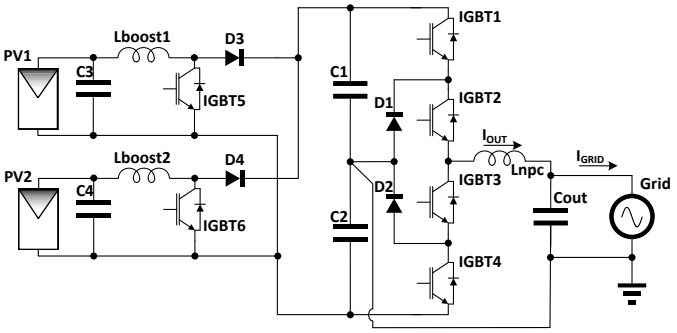

Fig. 5. Double-boost + NPC half-bridge converter

Some simulations by means of the PSIM™ Thermal Module software have been performed in order to compare the efficiency of the GCC circuit with that of the double-boost converter. The IGBTs selected for the simulations are the Infineon IKW15N120H3 and the diodes the Infineon IDP18E120. Both circuits have been simulated using the same IGBTs and diodes under the three unbalance scenarios described above.

In table 1 only the power losses in the switches and in the inductance of both dc-dc stages under comparison are shown, since the losses of the NPC inverters are identical in both cases. Note that both NPC inverters work from the same dc voltage of 800 V, managing the same power.

	Double-boost dc-dc	**GCC**
Balanced generation	39.7 W	4.1 W
Unbalanced generation	46.4 W	26.4 W
Severely unbalanced generation	69.5 W	59 W

Table 1. Power losses in the dc-dc stage

The GCC converter has lower power losses than the double-boost in all the scenarios under study, since it only manages the power difference between both strings. Note that the losses strongly depend on the degree of unbalance, being the higher, the higher the unbalance. The double-boost scheme has a lower variation of the losses when the unbalance scenario is changing. The simulations indicate that the GCC has a higher efficiency than the more common double-boost solution.

V. CONTROL STRUCTURE

The control structure proposed for the NPC+GCC is shown in figure 6. It is worth pointing out that the description of the converter dynamic model and the adjustment of the controllers is beyond the scope of this paper, but a short description of the control structure is provided. The control of the NPC inverter and of the GCC converter is independent: each one has its own current and voltage regulators and PWM modulator. The inverter regulates the total dc-link voltage (V_{PV1}+V_{PV2}), and the GCC regulates the voltage in the string PV2 (V_{PV2}). In this way both PV voltages are independently controlled.

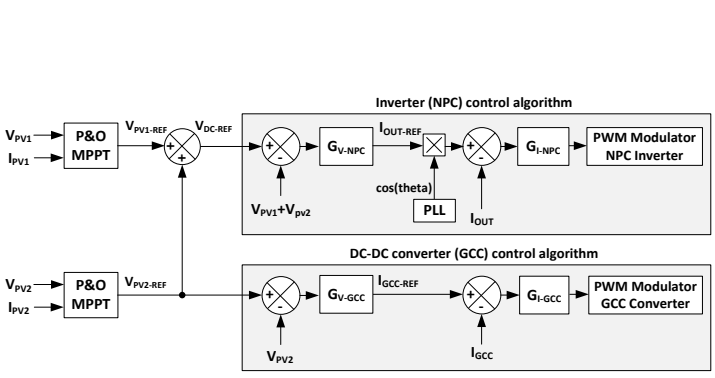

a)

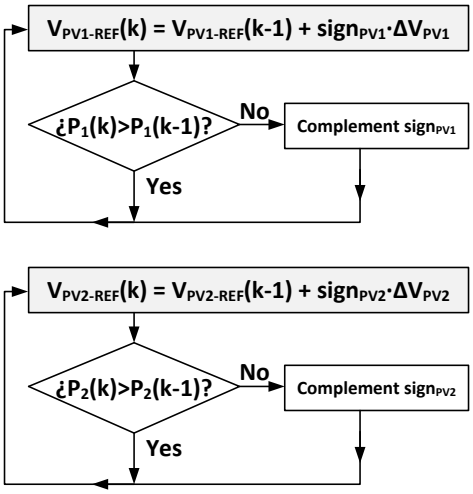

b)

Fig. 6. Control structure and double-MPPT algorithm of the NPC+GCC converter. a) Current and voltage loops, b) double-MPPT P&O algorithm

The voltage regulator of the NPC inverter ($G_{V\text{-}NPC}$) modifies the reference for the output current amplitude, $I_{OUT\text{-}REF}$, in order to regulate the total input voltage ($V_{DC}=V_{PV1}+V_{PV2}$) at the desired level. A Phase-Locked Loop (PLL) module ensures that the output current phase matches the grid voltage phase. The PLL is based on an SRF-PLL, as reported in [22].

The GCC voltage regulator ($G_{V\text{-}GCC}$) adjusts the GCC current reference ($I_{GCC\text{-}REF}$) in order to set the voltage V_{PV2} at the desired level. Since the current through the GCC inductor is the current difference between PV strings, the GCC transfers energy between strings.

Regarding the structure of the regulators, for the GCC voltage and current regulators Proportional-Integrator (PI) structures are chosen. For the NPC current regulator ($G_{I\text{-}NPC}$) a P+Resonant regulator structure is selected [23], whereas a PI regulator is used for the input voltage regulator ($G_{V\text{-}NPC}$). More details about the design of the regulators in single-phase grid-tied PV inverters can be found in [23]. The continuous-time expressions of those regulators are given by equations (7) to (10). They are implemented digitally after discretization with the Tustin method at a sampling frequency of *32kHz*.

$$G_{I-GCC}(s) = \frac{-15}{s} \cdot \frac{1 + {}^{s}/_{200}}{1 + {}^{s}/_{30000}} \tag{7}$$

$$G_{V-GCC}(s) = \frac{1 + {}^{s}/_{5}}{s} \tag{8}$$

$$\begin{aligned} G_{I-NPC}(s) = 0.05 &+ \frac{10 \cdot s}{s^2 + 7 \cdot s + (2 \cdot \pi \cdot 50)^2} \\ &+ \frac{25 \cdot s}{s^2 + 21 \cdot s + (2 \cdot \pi \cdot 150)^2} \\ &+ \frac{30 \cdot s}{s^2 + 35 \cdot s + (2 \cdot \pi \cdot 250)^2} \\ &+ \frac{35 \cdot s}{s^2 + 49 \cdot s + (2 \cdot \pi \cdot 350)^2} \end{aligned} \tag{9}$$

$$G_{V-NPC}(s) = -4 \cdot \frac{1 + {}^{s}/_{20}}{s} \tag{10}$$

The MPPT algorithm is a double-MPPT based on the Pertub&Observe (P&O) technique with a fixed step size [24-26], which modifies the references for both PV sources voltages: $V_{PV1\text{-}REF}$ and $V_{PV2\text{-}REF}$. As it is observed from the control structure of figure 6.a, the algorithm is formed by a pair of independent P&O algorithms. The flowchart of the MPPT algorithm is shown in figure 6.b. Two variables, $sign_{PV1}$ and $sign_{PV2}$, are used by the algorithm. Those variables can take the values +1 or -1, which can be changed at each interaction of the MPPT algorithm.

The MPPT step size has been chosen of 2V, which represents the 0.5% of the MPP voltage. Lower steps works worse because the noise affects the power measurement. The chosen step size results from a compromise between MPPT accuracy and noise in the experimental prototype.

VI. Experimental results

A prototype of a *5kW* NPC+GCC PV inverter has been implemented to validate the concept. The components and values of the prototype are the following:

- IGBT1 to IGBT4 and diodes D1to D2: module Microsemi APTGL60TL120T3G
- IGBT5 and IGBT 6: IR G4PH40KD
- DC-link capacitors: C1=*3 mF*, C2=*3 mF*
- Output LC filter: Lnpc=*2mH*, Cout=*9.4µF*
- GCC inductor: Lgcc=*15mH*
- Switching frequency: *16kHz*
- Sampling frequency: *32kHz*
- MPPT update period: *300ms*
- MPPT step size: *2V*

The control of the converter is performed by a Texas Instruments TMS230F28335 digital signal processor. For the experimental setup the converter is connected to a grid of $230V_{rms}$ and *50Hz*. The photovoltaic (PV) modules are emulated by means of two PV-source emulators. The emulated PV-sources are 2 strings each one composed by 14 230W PV modules model SLK60P6L from the manufacturer Siliken connected in series.

In order to test the performance of the converter regarding leakage currents, a parasitic capacitance must be emulated. The capacitance to ground of any terminal of the PV strings is estimated as *100nF*. These capacitances are emulated by placing film capacitors of *100nF/1100 V* connected between the terminals P, Z and N of the converter and ground (see figure 4). Each PV-source emulator is configured as 14 PV modules connected in series, with an irradiation of $1000W/m^2$ and *T=25ºC.*, with a maximum output power of *2.93kW* at an irradiation level of $1000W/m^2$ and *T=25ºC.*

The waveforms of the output voltage of the inverter before filtering, V_{INV}, and the current through L_{npc}, I_{OUT}, are shown in figure 7.a. The operation point is: V_{PV1}=448.2 V, I_{PV1}=3.6 A, P_{PV1}=1614 W, V_{PV2}=446 V, I_{PV2}=3.81 A, P_{PV2}=1699 W, I_{gcc}=0 A, P_{PV}=3313 W. Figure 7.b shows the grid voltage and the current I_{grid}. The THD of the grid voltage in the lab is THD_V=1.46%, whereas the measured THD of the output current is *THDi=2.9%*. Figure 7.c depicts the low-frequency FFT of the grid current, and figure 7.d depicts the first frequency band of the high-frequency harmonics of I_{grid}. The low frequency harmonics have been measured by means of a low frequency Fluke 43B Power Quality Analyzer (DC to 3.5 kHz) and a LEM PR 30 current probe (DC to 100 kHz), capable of measuring the DC level of the grid current. The high frequency harmonics have been obtained by means of a FRA5097 frequency response analyzer (0.1 mHz to 15 MHz).

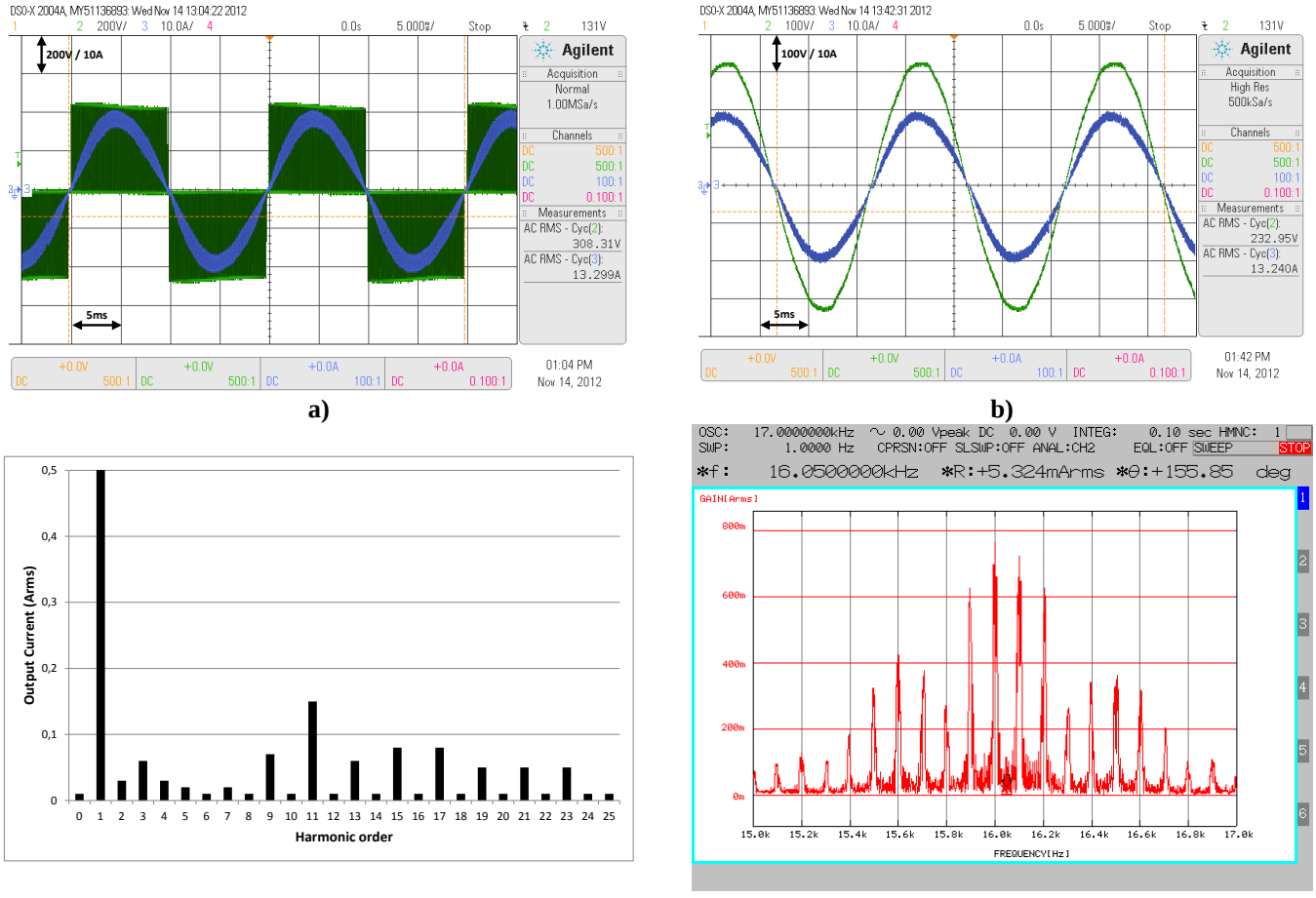

Fig. 7. a) Inverter output voltage before filtering (green trace) and current through Lnpc (blue trace). b) Grid voltage (green trace) and current injected by the inverter to the grid, I_{grid} (blue trace). The irradiation level in strings PV1 and PV2 is 1000W/m^2; c) Low frequency FFT of I_{grid}; d) First frequency band of the high frequency harmonics of I_{grid}

The leakage current is produced by the voltages from the poles of the PV strings to ground. As the leakage current flows through capacitances, it is mainly affected by the voltage ripple and its frequency. In the NPC+GCC topology the voltage ripple in the PV modules is mainly of *50Hz*, since it is a half-bridge inverter topology with the neutral connected to the midpoint of the input voltage. The Fast Fourier Transform (FFT) of the common-mode voltage and of the leakage current has been obtained by means of a frequency response analyzer NF FRA5097, as shown in Figures 8.a and 8.b, respectively. It is observed that the harmonic contents of this voltage is very low (lower than 6 V at V_{PV}≈450V) and at low frequency. The *50Hz* component of the leakage current has a very low RMS value, lower than *2mA*. The harmonics placed at higher frequencies are even lower. The total

RMS value of the leakage current to earth is around *2.1 mA_{RMS}*. According to the German DIN VDE 0126-1-1 standard, the leakage current value is limited to *300 mA_{RMS}*. This result confirms that the NPC+GCC topology is suitable for transformerless operation in photovoltaic power plants.

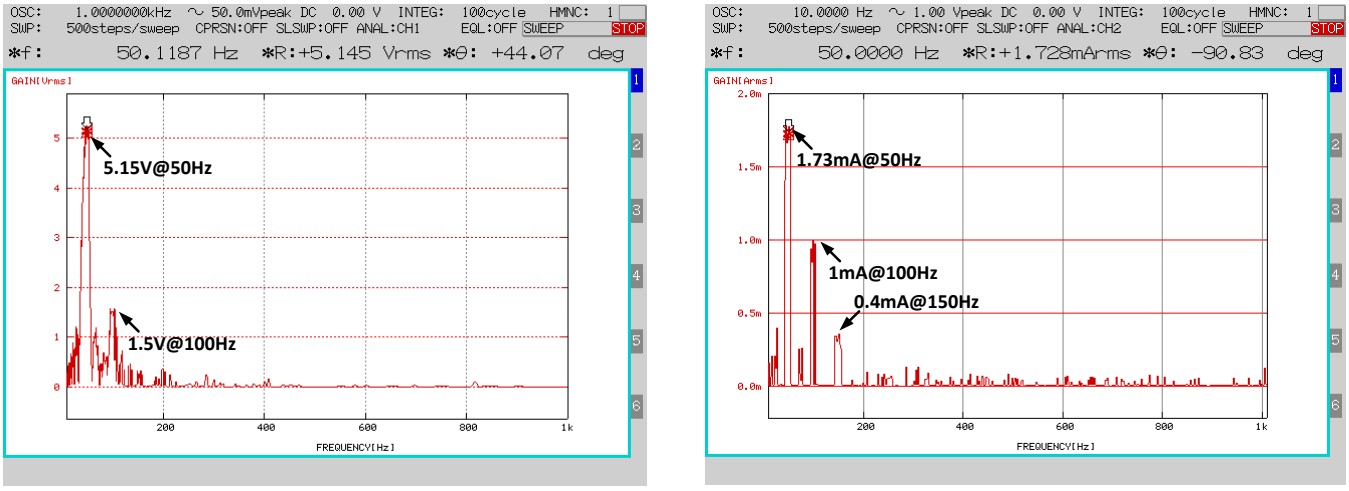

a) **b)**

Fig. 8.a) FFT of the common-mode voltage. b) FFT of the leakage current

In order to test the double-MPPT performance of the proposed converter, the PV-source emulators are configured as shown below, so that the partial shadowing in a photovoltaic power plant can be emulated:

- Emulator PV1: *600W/m^2* (V_{MPP}*=393.8V;* I_{MPP}*=4.51A*)
- Emulator PV2: *800W/m^2* (V_{MPP}*=394.5V*; I_{MPP}*=6.07A*)

In a first test the GCC converter is disconnected in order to show the MPP mismatch under partial shadowing. The inverter runs with a classical Perturb&Observe MPPT algorithm working from the measurement of total input voltage ($V_{PV}=V_{PV1}+V_{PV2}$) and from the current through both the strings, which are working in series when the GCC is disconnected. In figure 9.a the evolution of the experimental I-V values are plotted over the emulated characteristic curves of both strings. It is observed how the current of the string PV2 is limited by PV1, which is under a lower irradiation level, thus limiting the power obtained from the string PV2. In steady state the power obtained from PV1 is P_{PV1}*=1.753W* (P_{MPP}*=1.776W*), and the power obtained from PV2 is P_{PV2}*=1.990W* (P_{MPP}*=2.395W*). The overall extracted power is P_{PV}*=3.743W*, whereas the maximum power that can be extracted is P_{MPP}*=4.171W*. The power loss can be clearly observed in figure 9.b, which depicts the evolution of the experimental P-V values and the emulated P-V characteristics of the strings.

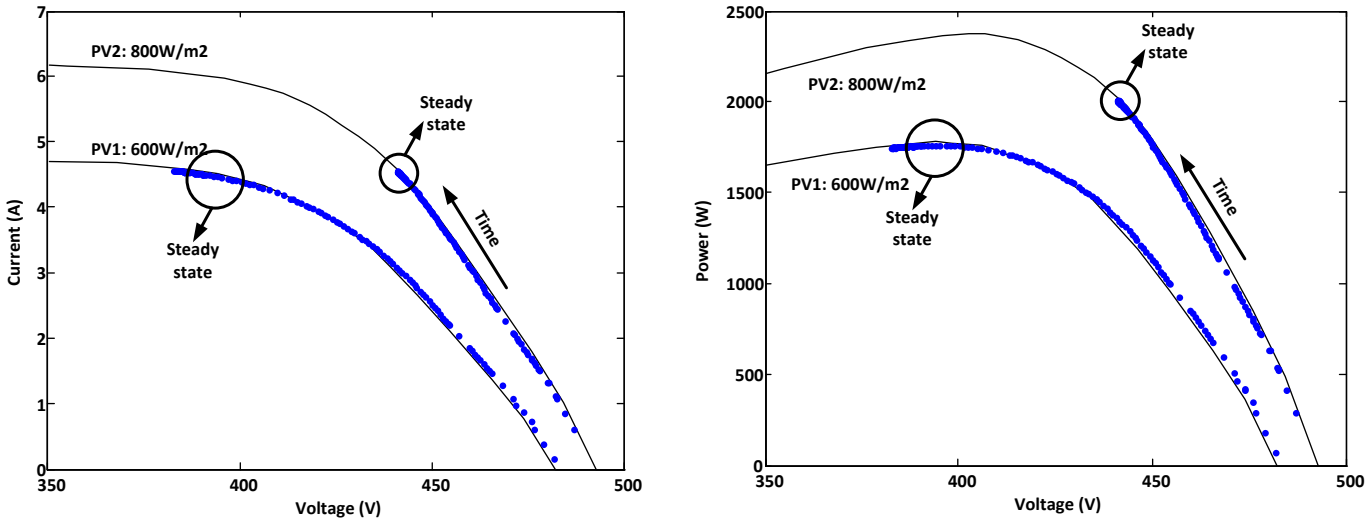

a) **b)**

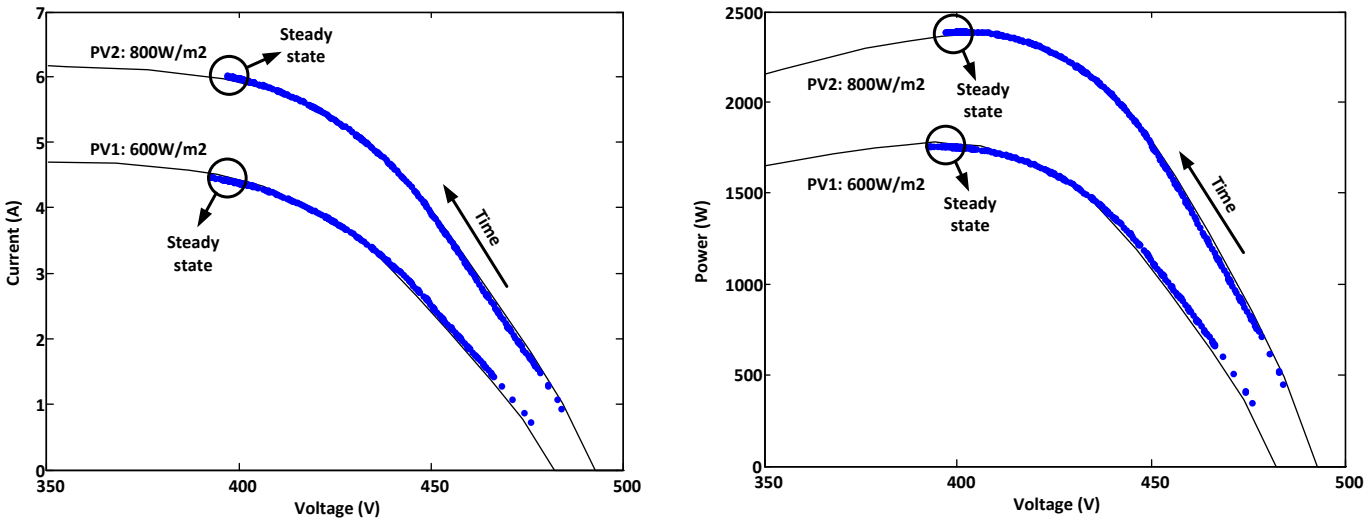

Fig. 9. a) I-V evolution with the GCC disconnected. b) P-V evolution with the GCC disconnected. c)I-V evolution with the GCC enabled. d) P-V evolution with the GCC enabled. Lines: characteristic curves. Dots: measured points.

Figures 9.c and 9.d shows the performance of the GCC working in conjunction with the double-MPPT algorithm. In figure 9.c it is observed that the currents in PV1 and PV2 are different in steady state, resulting in the extraction of the maximum power from both PV sources (see figure 9.d). As a result, the overall power extracted from both strings is increased: $P_{PV1}=1.755W$, $P_{PV2}=2.384W$, $P_{PV}=P_{PV1}+P_{PV2}=4.139W$. The power from PV2 is higher than without GCC circuit, because this circuit allows the current through string PV2 to be different to that through PV1. From the P-V evolution shown in figure 9.d it is observed that in steady state the individual MPPs of both strings are practically reached when connecting the GCC circuit.

Note that the increment in the generated power (from 3.743W to 4.139W, yielding an increment of 396W) achieved by the GCC circuit is much higher than the additional power losses in the GCC (19W) in the unbalance situation corresponding to figure 9. It can be concluded that the proposed converter increases the overall efficiency of the energy injected to the grid.

The Total Harmonic Distortion of the inverter output current (THDi) has been evaluated under an ideal grid voltage (THDv=0%), using a linear AC power supply PACIFIC POWER 360-AMX. The inverter has been fed by the PV emulators and variations of irradiance have been applied. The THDi under equal irradiation levels in both PV emulators is shown in table 2.

Irradiance (W/m^2)	PV1 power (kW)	PV2 power (kW)	Output power (kW)	THDi (%)
200	0.54	0.54	1.03	3.15
400	1.13	1.14	2.17	3.01
600	1.73	1.75	3.32	2.90
800	2.33	2.35	4.45	3.15
1000	2.91	2.92	5.56	3.50

Table 2. THDi(%) for several irradiation levels. Same irradiation levels at PV1 and PV2

However, when the irradiance at the strings PV1 and PV2 is unbalanced, the THDi is slightly affected, because the three-level voltage provided by the NPC inverter before filtering, V_{INV}, has different values of the positive and negative amplitudes. Nevertheless, it will be shown in the following that the THDi of the proposed topology is inside the maximum limits of the IEEE1547 standard in spite of an important irradiance unbalance at both PV sources. To show the influence of this unbalance, the irradiance at string PV1 is fixed at $500W/m^2$, and the irradiance at string PV2 is varied in the range $200W/m^2$ to $1000W/m^2$. The data for the THDi is shown in table 3. It is observed that the THDi is lower than 5% in all cases, as required by the IEEE1547. It is observed in table 3 that the higher the unbalance, the higher is the THDi. In the experimental results the maximum unbalance in the PV generators has been limited to a maximum irradiation difference of $500W/m^2$.

PV2 Irradiance (W/m^2)	Power PV1 (kW)	Power PV2 (kW)	Output power (kW)	THDi(%)
200	1.44	0.54	1.85	3.32
400	1.44	1.13	2.43	2.93
600	1.44	1.74	3.01	2.94

800	1.44	2.35	3.58	2.97
1000	1.44	2.90	4.08	3.22

Table 3. THDi(%) for several irradiation levels. Different irradiation levels at PV1 and PV2. PV1 at a constant irradiation level of *500W/m²*, PV2:*200W/m²* to *1000W/m²*

The waveforms of the grid voltage and grid injected current at different operation conditions are depicted in figure 10. In figure 10.a it is shown the grid voltage and the grid injected current for an identical irradiance level at PV1 and PV2 of *200 W/m²*. The injected power in this case is *1 kW*, whereas the THDi is 3.15%. In figure 10.b it is shown the first frequency band of the high frequency harmonics of the grid current at a low irradiance level (*200 W/m²* at both strings). Figures 10.c and 10.d are analog to 10.a and 10.b, respectively, corresponding to the test of the proposed topology under severely unbalanced conditions (PV1:*200W/m²*, PV2:*800W/m²*). The voltage mismatch in the PV strings is *46 V* (V_{PV1}=*362V*, V_{PV2}=*408V*), whereas the measured THDi is *4.08%*.

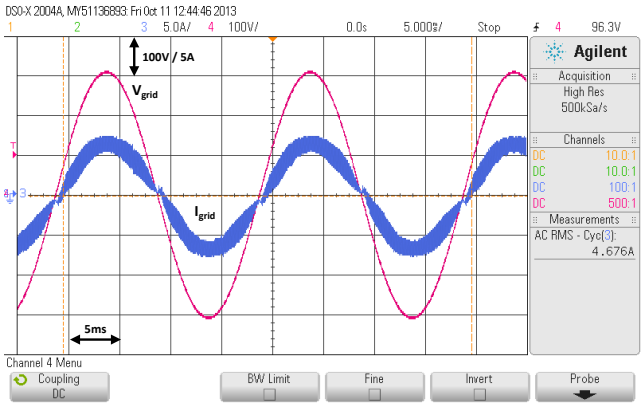

a)

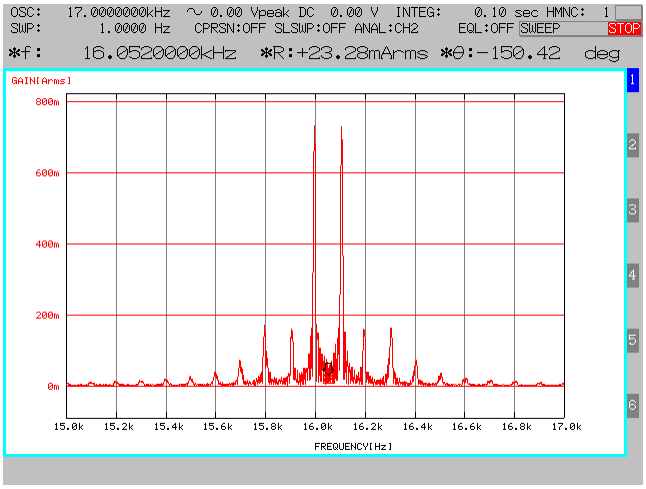

b)

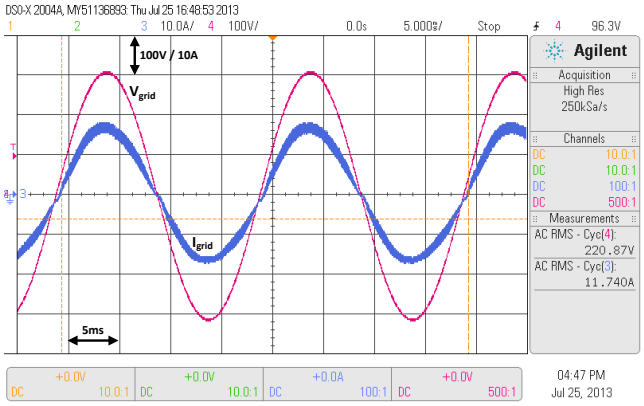

c)

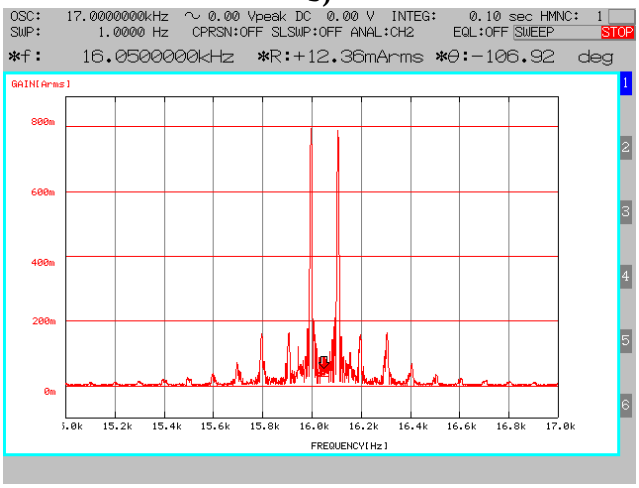

d)

Fig. 10. Grid voltage (pink trace) and grid current, I_{grid} (blue trace) under extreme operating conditions. a) Low irradiance level (PV1:*200 W/m²*; PV2:*200 W/m²*); b) First frequency band of the high frequency harmonics of I_{grid} at a low irradiance level (PV1:*200 W/m²*; PV2:*200 W/m²*); c) Severely unbalanced irradiation conditions (PV1:*200 W/m²*; PV2:*800 W/m²*); d) First frequency band of the high frequency harmonics of I_{grid} at a severely unbalanced irradiation conditions (PV1:*200 W/m²*; PV2:*800 W/m²*).

The low frequency FFT of the grid current in the conditions of figure 10, from DC up to the 25th harmonic, is shown in figure 11. It is verified that the standard IEEE1547 is complied, both regarding the limits for the harmonics and the limits for DC current injection (lower than 108 mA_{RMS} = 0.5% of the nominal output current).

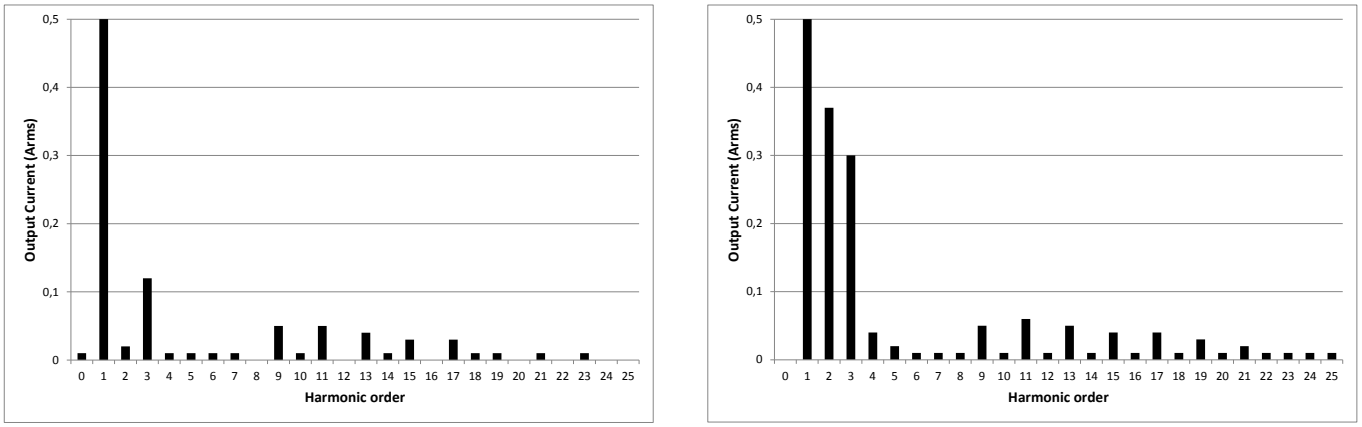

a) **b)**

Fig. 11. a) Low frequency FFT of for a low irradiance level (PV1:*200 W/m*^{2}; PV2:*200 W/m*^{2}; b) Low frequency FFT for severely unbalanced irradiation conditions (PV1:*200 W/m*^{2}; PV2:*800 W/m*^{2});

The efficiency of the NPC+GCC converter has been measured. The efficiency is calculated as the ratio between the output power and the sum of the powers extracted from both PV sources, following (9).

$$\eta(\%) = 100 \cdot \frac{P_{OUT}}{P_{PV1} + P_{PV2}} \qquad (9)$$

The efficiency is measured at different output power levels in order to obtain the value of the European efficiency, calculated as shown in (10), where $\eta_{i_{\%}}$ is the efficiency at i% of the converter output rated power [27].

$$\eta_{EURO} = 0.03 \cdot \eta_{5\%} + 0.06 \cdot \eta_{10\%} + 0.13 \cdot \eta_{20\%} + 0.10 \cdot \eta_{30\%} + 0.48 \cdot \eta_{50\%} + 0.20 \cdot \eta_{100\%} \qquad (10)$$

The measured efficiency vs. power data with an identical power level in both PV sources is shown in figure 12.a. The European efficiency is 95.7%, and the maximum efficiency is 96.2%.

The efficiency is also affected by the unbalance, as it is depicted in figure 12.b. In this figure the input power of the input PV1 is fixed at different values and the power of input PV2 is varied. The converter efficiency has been plotted for different values of the power from PV1. It is observed that the dispersion of efficiency values is lower than 1% in a wide range.

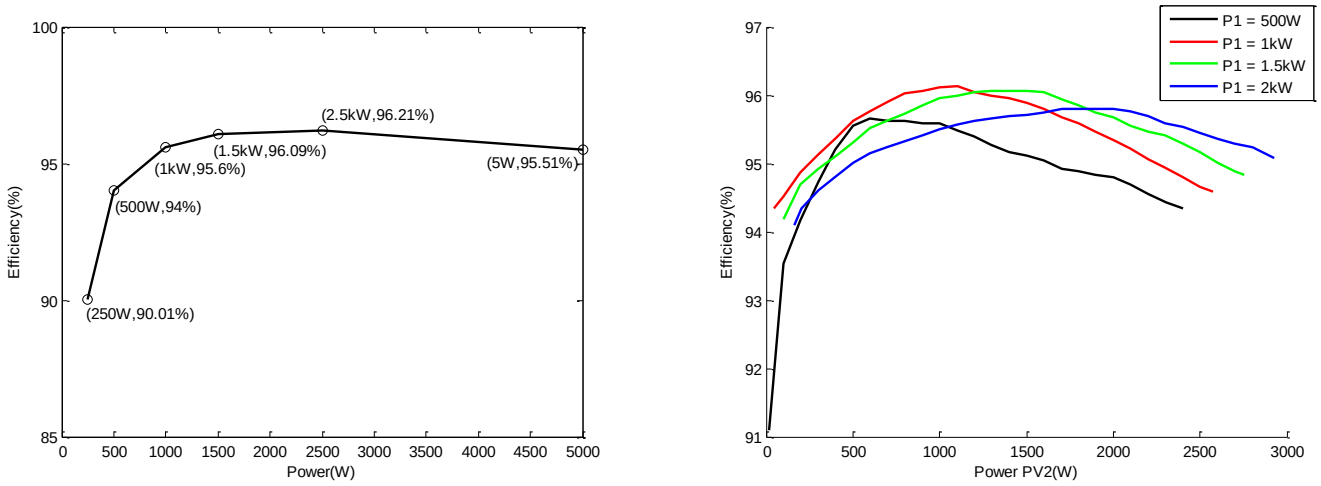

a) **b)**

Fig. 12. a) Efficiency versus output power. Identical operating point of both PV sources b) Efficiency versus input power in PV1 and PV2

VII. CONCLUSION

A new topology of single-phase transformerless PV inverter capable of operating from two PV sources has been presented. To test the performance of the NPC+GCC topology a *5kW* prototype has been implemented and tested. The experimental results show that the common mode voltage at the PV source terminals doesn´t contain high frequency components, so that the leakage

currents to ground are minimized. Therefore, the inverter is suitable for transformerless operation.

Besides, with a minimum quantity of additional elements, the topology includes a dc-dc converter that allows the independent tracking of the MPP of both PV strings connected at the input. A double MPPT algorithm has been proposed to achieve that task, resulting in an improvement of the PV facility efficiency under partial shadowing conditions. This improvement has been tested in the laboratory using two photovoltaic emulators.

The European efficiency takes a value around 96%, whereas the efficiency dispersion at a power mismatch of both PV sources is lower than 1%.

VIII. Acknowledgment

This work is supported by the Spanish Ministry of Science and Innovation under grants ENE2009-13998-C02-02 and ENE2012-37667-C02-01.

References

[1] H. Bevrani, A. Ghosh, and G. Ledwich, "Renewable energy sources and frequency regulation: survey and new perspectives," *Renewable Power Generation, IET*, vol. 4, no. 5, pp. 438-457, Sept.2010.

[2] J. Zhu, R. Brundlinger, T. hlberger, T. R. Betts, and R. Gottschalg, "Optimised inverter sizing for photovoltaic systems in high-latitude maritime climates," *Renewable Power Generation, IET*, vol. 5, no. 1, pp. 58-66, Jan.2011.

[3] E. I. Amoiralis, M. A. Tsili, and A. G. Kladas, "Power Transformer Economic Evaluation in Decentralized Electricity Markets," *Industrial Electronics, IEEE Transactions on*, vol. 59, no. 5, pp. 2329-2341, May2012.

[4] L. Bowtell and A. Ahfock, "Direct current offset controller for transformerless single-phase photovoltaic grid-connected inverters," *Renewable Power Generation, IET*, vol. 4, no. 5, pp. 428-437, Sept.2010.

[5] I. Patrao, E. Figueres, F. González-Espín, and G. Garcerá, "Transformerless topologies for grid-connected single-phase photovoltaic inverters," *Renewable and Sustainable Energy Reviews*, vol. 15, no. 7, pp. 3423-3431, Sept.2011.

[6] S. V. Araujo, P. Zacharias, and B. Sahan, "Novel grid-connected non-isolated converters for photovoltaic systems with grounded generator," *PESC 2008. IEEE Power Electronics Specialists Conference*, pp. 58-65, June2008.

[7] S. B. Kjaer, J. K. Pedersen, and F. Blaabjerg, "A review of single-phase grid-connected inverters for photovoltaic modules," *IEEE Transactions on Industry Applications*, vol. 41, no. 5, pp. 1292-1306, Sept.2005.

[8] H. B. Puttgen, P. R. MacGregor, and F. C. Lambert, "Distributed generation: Semantic hype or the dawn of a new era?," *Power and Energy Magazine, IEEE*, vol. 1, no. 1, pp. 22-29, Jan.2003.

[9] H. Nian and R. Zeng, "Improved control strategy for stand-alone distributed generation system under unbalanced and non-linear loads," *Renewable Power Generation, IET*, vol. 5, no. 5, pp. 323-331, Sept.2011.

[10] M. Thomson and D. G. Infield, "Impact of widespread photovoltaics generation on distribution systems," *Renewable Power Generation, IET*, vol. 1, no. 1, pp. 33-40, Mar.2007.

[11] E. Karatepe, S. Syafaruddin, and T. Hiyama, "Simple and high-efficiency photovoltaic system under non-uniform operating conditions," *Renewable Power Generation, IET*, vol. 4, no. 4, pp. 354-368, July2010.

[12] Y.-J. Wang and P.-C. Hsu, "Analytical modelling of partial shading and different orientation of photovoltaic modules," *Renewable Power Generation, IET*, vol. 4, no. 3, pp. 272-282, May2010.

[13] O. Lopez, F. D. Freijedo, A. G. Yepes, P. Fernandez-Comesaa, J. Malvar, R. Teodorescu, and J. Doval-Gandoy, "Eliminating Ground Current in a Transformerless Photovoltaic Application," *IEEE Transactions on Energy Conversion*, vol. 25, no. 1, pp. 140-147, Mar.2010.

[14] R. Petrella, N. Buonocunto, A. Revelant, and P. Stocco, "DC bus voltage equalization in single-phase split-capacitor three-level neutral-point-clamped half-bridge inverters for PV applications," *Applied Power Electronics Conference and Exposition (APEC), 2011 Twenty-Sixth Annual IEEE*, pp. 931-938, Mar.2011.

[15] M. Lin, T. Kerekes, R. Teodorescu, J. Xinmin, D. Floricau, and M. Liserre, "The high efficiency transformer-less PV inverter topologies derived from NPC topology," *EPE '09. 13th European Conference on Power Electronics and Applications*, pp. 1-10, 2009.

[16] M. C. Cavalcanti, A. M. Farias, K. C. Oliveira, F. A. S. Neves, and J. L. Afonso, "Eliminating Leakage Currents in Neutral Point Clamped Inverters for Photovoltaic Systems," *Industrial Electronics, IEEE Transactions on*, vol. 59, no. 1, pp. 435-443, Jan.2012.

[17] T. Kerekes, R. Teodorescu, P. Rodriguez, G. Vazquez, and E. Aldabas, "A new high-efficiency single-phase transformerless PV inverter topology," *IEEE Transactions on Industrial Electronics*, no. 99 2009.

[18] Y. H. Ji, D. Y. Jung, J. G. Kim, J. H. Kim, T. Lee, and C. Y. Won, "A Real Maximum Power Point Tracking Method for Mismatching Compensation in PV Array under Partially Shaded Conditions," *Power Electronics, IEEE Transactions on*, vol. PP, no. 99, p. 1, 2000.

[19] W. Tsai-Fu, C. Chih-Hao, L. Li-Chiun, and K. Chia-Ling, "Power Loss Comparison of Single- and Two-Stage Grid-Connected Photovoltaic Systems," *Energy Conversion, IEEE Transactions on*, vol. 26, no. 2, pp. 707-715, June2011.

[20] T. Shimizu, M. Hirakata, T. Kamezawa, and H. Watanabe, "Generation control circuit for photovoltaic modules," *IEEE Transactions on Power Electronics*, vol. 16, no. 3, pp. 293-300, May2001.

[21] G. Vazquez, T. Kerekes, A. Rolan, D. Aguilar, A. Luna, and G. Azevedo, "Losses and CMV evaluation in transformerless grid-connected PV topologies," *ISIE 2009. IEEE International Symposium on Industrial Electronics*, pp. 544-548, July2009.

[22] F. Gonzalez-Espin, E. Figueres, and G. Garcera, "An Adaptive Synchronous-Reference-Frame Phase-Locked Loop for Power Quality Improvement in a Polluted Utility Grid," *Industrial Electronics, IEEE Transactions on*, vol. 59, no. 6, pp. 2718-2731, June2012.

[23] M. Ciobotaru, R. Teodorescu, and F. Blaabjerg, "Control of single-stage single-phase PV inverter," *Power Electronics and Applications, 2005 European Conference on*, p. 10, 2000.

[24] R. A. Mastromauro, M. Liserre, and A. Dell'Aquila, "Control Issues in Single-Stage Photovoltaic Systems: MPPT, Current and Voltage Control," *Industrial Informatics, IEEE Transactions on*, vol. 8, no. 2, pp. 241-254, May2012.

[25] F. Delfino, G. B. Denegri, M. Invernizzi, and R. Procopio, "Feedback linearisation oriented approach to Q-V control of grid connected photovoltaic units," *Renewable Power Generation, IET*, vol. 6, no. 5, pp. 324-339, Sept.2012.

[26] K. Ishaque and Z. Salam, "A review of maximum power point tracking techniques of PV system for uniform insolation and partial shading condition," *Renewable and Sustainable Energy Reviews*, vol. 19, no. 0, pp. 475-488, Mar.2013.

[27] M. Valentini, A. Raducu, D. Sera, and R. Teodorescu, "PV inverter test setup for European efficiency, static and dynamic MPPT efficiency evaluation," *Optimization of Electrical and Electronic Equipment, 2008. OPTIM 2008. 11th International Conference on*, pp. 433-438, May2008.